

Serveur Académique Lausannois SERVAL [serval.unil.ch](http://serval.unil.ch)

## Author Manuscript

Faculty of Biology and Medicine Publication

This paper has been peer-reviewed but does not include the final publisher proof-corrections or journal pagination.

Published in final edited form as:

**Title:** CRISPR-mediated kinome editing prioritizes a synergistic combination therapy for FGFR1-amplified lung cancer.

**Authors:** Yang Z, Liang SQ, Yang H, Xu D, Bruggmann R, Gao Y, Deng H, Berezowska S, Hall SRR, Marti TM, Kocher GJ, Zhou Q, Schmid RA, Peng RW

**Journal:** Cancer research

**Year:** 2021 Mar 8

**DOI:** [10.1158/0008-5472.CAN-20-2276](https://doi.org/10.1158/0008-5472.CAN-20-2276)

In the absence of a copyright statement, users should assume that standard copyright protection applies, unless the article contains an explicit statement to the contrary. In case of doubt, contact the journal publisher to verify the copyright status of an article.

## CRISPR-mediated kinome editing prioritizes a synergistic combination therapy for *FGFR1*-amplified lung cancer

Zhang Yang<sup>1,2¶</sup>, Shun-Qing Liang<sup>1,2¶§</sup>, Haitang Yang<sup>1,2</sup>, Duo Xu<sup>1,2</sup>, Rémy Bruggmann<sup>3</sup>, Yanyun Gao<sup>1,2</sup>, Haibin Deng<sup>1,2</sup>, Sabina Berezowska<sup>4</sup>, Sean R. R. Hall, Thomas M. Marti<sup>1,2</sup>, Gregor J. Kocher<sup>1,2</sup>, Qinghua Zhou<sup>5</sup>, Ralph A. Schmid<sup>1,2\*</sup>, Ren-Wang Peng<sup>1,2\*</sup>

<sup>1</sup>Division of General Thoracic Surgery, <sup>2</sup>Department for BioMedical Research (DBMR), Inselspital, Bern University Hospital, University of Bern, Switzerland;

<sup>3</sup>Interfaculty Bioinformatics Unit and Swiss Institute of Bioinformatics, University of Bern, Bern, Switzerland;

<sup>4</sup>Institute of Pathology, University of Bern, Bern, Switzerland;

<sup>5</sup>Lung Cancer Center, West China Hospital, Sichuan University, Chengdu, China;

¶Equal contribution to this study

§Current address: University of Massachusetts Medical School, Worcester, MA 01605, USA

**Running title:** A synergy between FGFR and PLK1 inhibitors

**Keywords:** Lung cancer, *FGFR1* amplification, CRISPR screen, PLK1, synergistic combination therapy

**Correspondence:** Ren-Wang Peng, PhD, Division of General Thoracic Surgery, Department for BioMedical Research (DBMR), Inselspital, Bern University Hospital, University of Bern, Murtenstrasse 50, 3008 Bern, Switzerland. Phone: +41 31 632 40 81  
Email: Renwang.Peng@insel.ch

Ralph A. Schmid, MD, Division of General Thoracic Surgery, Department for BioMedical Research (DBMR), Inselspital, Bern University Hospital, University of Bern, Murtenstrasse 50, 3008 Bern, Switzerland. Phone: +41 31 632 23 64; Email: Ralph.Schmid@insel.ch

### **Conflict of interest:**

The authors declare no potential conflicts of interest.

**This article contains supporting information and datasets.**

Abstract word count: 154  
Text word count: 5033  
Reference: 50  
Main figures: 6  
Supplementary figures: 7  
Supplementary Tables: 6  
Supplementary dataset: 3

## ABSTRACT

**Oncogenic activation of the fibroblast growth factor receptor (FGFR) pathway is frequent in lung and other cancers. However, due to drug resistance, pharmacological blockage of aberrant FGFR signaling has provided little clinical benefit in patients with *FGFR*-amplified tumors. The determining factors for the limited efficacy of FGFR-targeted therapy remain incompletely understood. In this study, we performed kinome-wide CRISPR/Cas9 loss-of-function screens in *FGFR1*-amplified lung cancer cells treated with an FGFR inhibitor. These screens identified PLK1 as a potent synthetic lethal target that mediates a resistance mechanism by overriding DNA damage and cell cycle arrest upon FGFR1 inhibition. Genetic and pharmacological antagonism of PLK1 in combination with FGFR inhibitor therapy synergized to enhance anti-proliferative effects and drove cancer cell death *in vitro* and *in vivo* through activation of the  $\gamma$ H2AX-CHK-E2F1 axis. These findings suggest a previously unappreciated role for PLK1 in modulating FGFR1 inhibitor sensitivity and demonstrate a synergistic drug combination for treating *FGFR1*-amplified lung cancer.**

### Significance:

The identification of PLK1 as a potent synthetic lethal target for FGFR-targeted therapy provides an innovative rationale for the treatment of lung and other *FGFR1*-amplified cancers.

## INTRODUCTION

Fibroblast growth factor receptors (FGFRs) are receptor tyrosine kinases (RTKs) that regulate a variety of biological processes. FGFR signaling is frequently deregulated in cancers, most often because of gene amplifications, point mutations and fusions as well as of epigenetic and/or transcriptional deregulation (1). Compelling evidence has demonstrated the oncogenic potential of deregulated FGFR signaling in driving tumor growth (2,3). In particular, *FGFR1* amplifications occur in 10–20% of lung cancer, primarily squamous cell lung carcinoma (SQLC), making FGFR1 the biggest class of "druggable" targets in SQLC (4-6).

FGFRs as cancer targets provide novel opportunities for the development of precision therapy in *FGFR*-dependent malignancies (7-9). Preclinical and translational studies with FGFR tyrosine kinase inhibitors (FGFR-TKIs) have produced promising efficacy and manageable safety profiles in different cancer types, including *FGFR1*-amplified SQLC (10,11). However, FGFR-TKIs as single therapeutics benefit only a small fraction of patients, with reported clinical responses in approximately 11% of *FGFR1*-amplified SQLC (12,13). While these data support the notion that FGFR alterations are associated with tumor sensitivity to FGFR-TKIs (3), they also highlight the need to define biomarkers that can stratify patients who would benefit from FGFR-targeted therapy and, importantly, to identify complementary targets for combination treatment.

PLK1 is a ubiquitously expressed serine/threonine kinase vital for cell proliferation by regulating a multitude of mitotic events, i.e., mitotic entry, spindle formation, centrosome maturation, chromosome segregation and cytokinesis (14). In addition to the canonical function in governing mitotic progression, mounting evidence has also implicated non-mitotic roles for PLK1 in DNA damage responses by regulating ataxia-telangiectasia mutated (ATM)/CHK2 and ATM- and Rad3-Related (ATR)/CHK1 checkpoint activity (15-18). *PLK1* is highly expressed in malignant tumors but scarcely detectable in normal tissues and correlate with poor patient survival (19,20), indicating that targeting PLK1 can preferentially impair cancer cells while sparing normal cells. Notably, clinical trials have showed that selective PLK1 inhibitors are well tolerated by patients, but their utility as single agents is limited (21-24).

Functional genomics using pooled single-guide RNAs (sgRNAs) provides an unprecedented platform to identify therapeutic targets in cancer (25,26). In this study, we performed CRISPR/Cas9 screen that systematically assesses 764 human kinase genes that, when deleted, improve the efficacy of AZD4547, a selective FGFR-TKI under phase III clinical trials ([www.clinicaltrials.gov](http://www.clinicaltrials.gov)) in patients with *FGFR1*-amplified lung cancer (27,28). We showed that PLK1 is a potent synthetic lethal target in *FGFR1*-amplified lung cancer cells treated with FGFR-TKIs, and that combined inhibition of FGFR and PLK1 synergistically enhances cancer cell death *in vitro* and *in vivo*. Our work suggests a previously unappreciated role for PLK1 that determines FGFR1 inhibitor sensitivity and demonstrate a novel synergistic drug combination for the treatment of *FGFR1*-amplified lung cancer.

## MATERIALS AND METHODS

### **Cell culture and reagents**

*FGFR1*-amplified (H520, H1581, H1703, HCC95) and wild-type (PC-9, H1650, H1993, H2228, H226, H3122, and H522) lung cancer cells, untransformed normal cells (HFBN1 and BEAS-2B) are listed in Table S1. Cells were authenticated by DNA fingerprinting using highly-polymorphic short tandem repeat (STR) analysis, regularly confirmed free from mycoplasma contamination (Microsynth, Bern, Switzerland) and cultured in RPMI-1640 supplemented with 10% fetal bovine serum/FBS (Cat.#10270-106; Life Technologies, Grand Island, NY, USA) and 1% penicillin/ streptomycin solution (Cat. #P0781, Sigma-Aldrich) at 37°C with 95% air/5 % CO<sub>2</sub>. Small-molecule inhibitors targeting FGFR (AZD4547, BGJ398), PLK1 (BI2536, BI6267), microtubule (Paclitaxel) and other RTKs were purchased from Selleckchem (Houston, TX, USA) and shown in Table S2. FGFR inhibitor-resistant cells (H520R, H1703R) were generated by continuously exposure of parental cells to increasing doses of AZD4547 for at least six months.

### ***The sgRNA library and lentivirus production***

The pooled-sgRNA library (LentiCRISPRv2) targeting human kinome (25) was a gift from John Doench & David Root (Addgene, Cat. #75314). The lentivirus was produced as described (26,29). Briefly, five 10-cm dishes of H293T cells were plated at 30% confluence in antibiotic-free media (DMEM plus 10% FBS). Transfection was performed with MegaTran 1.0 (Cat. # TT200003; Origene, Rockville, MD, USA). For each dish, 9 µg of lentiCRISPR plasmid library, 0.9 µg of pVSVg (Addgene, Cat. #8584), 9 µg of psPAX2 (Addgene, Cat. #12260) and 54 µl of MegaTran 1.0 (Cat. # TT200003; Origene, Rockville, MD, USA) diluted in OptiMEM were mixed and added to the H293T cells. Medium was changed the next day and virus was collected 48 hours later by filtering through a 0.45 µm strainer.

### ***Pooled kinome-wide CRISPR/Cas9 screens***

The CRISPR screen was performed essentially as we described (29). Briefly, fifty millions of H520 cells were transduced via spin infection in triplicates with kinome-wide sgRNA lentiviral pool (MOI ~0.3). Cells were then selected with puromycin (1 µg/ml) for 3 days. Fifteen millions of transfected cells were saved for baseline (D0 treatment). The rest of survival cells were divided into two groups (4 x 15-cm dishes/group) following treatment with vehicle (PBS) or AZD4547 (1.5 µM) for 21 days. Cells were sub-cultured every three days and thirty millions of cells for each group were collected for DNA isolation at the end of the treatment.

### ***Genomic DNA sequencing and data analysis***

Genomic DNA was isolated from baseline, vehicle- and AZD4547-treated cells using the QIAamp DNA Blood Maxi Kit (Cat. #51192; QIAGEN, Hilden, Germany), followed by a two-step PCR procedure to amplify sgRNAs as previously described (29). For the first PCR, 18 separate 100 µl reactions were performed with 5 µg gDNA. The second PCR was done in a 100 µl reaction for 25 cycles by mixing 5 µl of the first PCR. All PCR primers are list in Table S3. The resulting PCR amplicons from the second PCR reactions were purified and sequenced by HiSeq

3000 (Illumina). Raw FASTQ files were demultiplexed and trimmed to contain the unique sgRNA sequence only. The number of reads for each sgRNA was quantified and normalized to total reads of all sgRNAs using the following equation: normalized counts of each sgRNA = (total reads per sgRNA in each sample / reads mapped to target library of each sample)  $\times 10^6 + 1$ . Student's t-test and Benjamini & Hochberg adjustment for multiple comparisons were used to determine p-values.

### ***Patient samples***

Surgically resected tumor specimens from patients with squamous cell lung carcinoma were obtained from Lung Cancer Center (LCC), Bern University Hospital. *FGFR1* amplifications in the tumors were analyzed by fluorescence in situ hybridization (FISH) at the Institute of Pathology, University of Bern. All human studies were conducted in accordance with Declaration of Helsinki and performed under the auspices of protocols approved by the institutional review board (KEK number: 042/15 and 200/2014), with written informed consent obtained from all patients.

### ***In vivo mouse study***

Mouse studies were approved by the Veterinary Office of Canton Bern, Switzerland, and conducted in accordance with Institutional Animal Care. All mouse experiments with human cell lines and clinical specimens from a patient with *FGFR1*-amplified SQLC (BE937T; male, 69 year-old; pT4, pN1, cM0; stage IIIA; no neoadjuvant treatment) were performed in age- and gender-matched NSG (NOD-*scid* *IL2Rγ<sup>null</sup>*). For H1703, H520 and EBC-1 xenografts, suspensions of 1 million cells (in PBS) mixed 1:1 with BD Matrigel Basement Membrane Matrix (Cat. #356231; Corning, NY, USA) were subcutaneously inoculated in left and right flanks. For the PDX model, tumor tissues were cut into small pieces (5  $\mu\text{m} \times 5 \mu\text{m}$ ) and inserted into a subcutaneous pocket. When tumors were palpable, mice were randomly assigned to treatment groups: 1) control; 2) BI2536 (40 mg/kg, i.v., once weekly) or BI6727 (5 mg/kg; i.p., daily); 3) AZD4547 (10 mg/kg, p.o., once daily); 4) Combination treatment (BI2536 or BI6727 plus AZD4547) administered at the same dose as single treatment. Treatment lasted for 3 weeks and tumor size was measured by caliper every three days. Tumor volume was calculated as follows: (length  $\times$  width<sup>2</sup>) / 2.

### ***Statistical analysis***

Statistical analyses were performed using GraphPad Prism 7.01 (GraphPad Software Inc.) unless otherwise indicated. All samples that met proper experimental conditions were included in the analysis and sample size was not pre-determined by statistical methods but rather based on preliminary experiments. Group allocation was performed randomly. In all studies, data represent biological replicates (n) and are depicted as mean  $\pm$  s.d. or mean  $\pm$  SEM as indicated in the figure legends. Comparison of mean values was conducted with unpaired, two-tailed Student's *t*-test, one-way ANOVA or two-way ANOVA with Tukey's multiple comparisons test as indicated in the figure legends. In all analyses, *P* values less than 0.05 were considered statistically significant.

## RESULTS

### Loss of function screens identify synthetic lethal targets in *FGFR1*-amplified lung cancer cells treated with an FGFR inhibitor

To identify genetic determinants underlying sensitivity to FGFR-targeted therapy, we performed kinome CRISPR/Cas9 knockout screens in *FGFR1*-amplified lung cancer cells (H520) (**Table S1**). H520 cells were infected at low multiplicity of infection (MOI) with the Broad Institute Brunello pooled sgRNAs library targeting 764 human kinase genes (4 sgRNAs/gene) (25) as we described (29). Infected cells selected by puromycin (3 days) were further treated with vehicle (PBS) and AZD4547 (**Table S2**) for 21 days. The sgRNAs were amplified by a two-step PCR procedure (**Table S3**) from genomic DNA isolated from the original library, vehicle- and AZD4547-treated H520 cells, referred to as H520\_B, H520\_V and H520\_F, respectively. Library presentations were determined by deep sequencing of the PCR amplicons from the individual samples and subsequent data analysis (**Figure 1A; Dataset S1**).

As expected, normalized sgRNA frequencies in H520\_B, H520\_V and H520\_F showed significant difference, whereas those of experimental replicates (n=3) in the same treatment group were highly reproducible (**Figure 1B; Fig. S1A, B**). We ranked individual sgRNAs based on log<sub>2</sub> fold-change (FC) in H520\_V versus (vs.) H520\_B and H520\_F vs. H520\_V (**Figure 1C; Dataset S2, S3**). We focused on negative selection (depleted sgRNAs) and prioritized target genes with multiple sgRNAs (n≥3) significantly depleted in H520\_V compared to H520\_B, and H520\_F relative to H520\_V, which nominated 22 candidates as proliferation-affecting (essential) genes (**Table S4**), and 12 kinase genes as potential synthetic lethal targets in AZD4547-treated cancer cells (**Table S5**).

Notably, the proliferation-affecting candidates (**Table S4**), including several cell-cycle kinase genes (*CDC7*, *CDK7* and *MVK*), substantially overlap with previously identified (30,31) cancer essential genes (**Fig. S1C**). The ability to successfully recover known essential genes validates the technical feasibility of our screen strategy and biological accountability of the results. Indeed, numerous candidate genes were amplified/deregulated in SQLC and/or of prognostic significance in patients with SQLC (**Fig. S1D, E**).

Importantly, our screens revealed a dozen of kinase genes (n=12), on the top (based on log<sub>2</sub>FC) including *CSNK2A1* (CK2α), *PIP4K2C* (PIP4ky), and *PLK1* (PLK1), whose loss of function by specific sgRNAs led to synthetic lethality with AZD4547 (**Figure 1C, D; Table S5**). Of particular note, PIP4ky is a substrate of mTOR (32) previously shown to be a synthetic lethal partner with *FGFR1* by a study using RNAi screens (33). CK2α is a serine/threonine kinase involved in a wide spectrum of biological processes including cell cycle regulation and DNA damage response (34,35) and, more relevant to our screen data, CK2α has been reported to regulate DNA double strand break repair by acting in concert with PLK1 (18). Premised on these observations and the advance of PLK1 inhibitors in clinical trials ([www.clinicaltrials.gov](http://www.clinicaltrials.gov)), we focused on PLK1 in the present study.

## **PLK1 blockage in combination with FGFR inhibitors synergistically enhances anti-proliferative effects and apoptosis in *FGFR1*-amplified lung cancer cells**

To validate PLK1 as a synthetic lethal target in *FGFR1*-amplified lung cancer cells, we first knocked down *PLK1* in H1703 and H520 cells by small interfering (si) RNAs. *PLK1* downregulation, confirmed by immunoblot analysis (**Table S6**), dramatically increased the sensitivity of H1703 and H520 cells to AZD4547, which was used at concentrations that effectively inhibited FGFR downstream effectors (p-AKT, p-ERK) (**Figure 2A**), causing enhanced anti-proliferative effects (**Figure 2B-D**) and significantly greater apoptosis (**Figure 2E**) in both cell lines compared to control siRNAs.

Pharmacological blockage of PLK1 by BI2536 (**Table S2**), a selective PLK1 inhibitor being clinically investigated (21,23), synergistically [combination index (CI) < 1] enhanced the anti-proliferative effect of AZD4547 in a panel of *FGFR1*-amplified lung cancer cells (H1703, H520, H1581 and HCC95) (**Figure 2F-I; Fig. S2A-D; Table S1**). The combinatorial effect was maintained when other small-molecule agents, e.g., the pan-FGFR inhibitor BGJ 398 (10,13) and BI6727 (Volasertib), a next-generation PLK1 inhibitor with improved pharmacokinetic profile (22) and being investigated in phase III clinical trials, were used (**Fig. S2E; Table S2**). In line with the results from our genetic study (**Figure 2E**), BI2536 in combination with AZD4547 significantly increased apoptotic death in H1703 and H520 cells (**Figure 2J, K; Fig. S2F, G**).

We next examined whether the effect of combined FGFR/PLK1 inhibition is related to FGFR1 protein expression. FGFR1 is highly expressed in *FGFR1*-amplified (H1703, H520, H1581), mildly or weakly expressed in non-*FGFR1*-amplified (H522, H226) and normal (HFBN-1) cells, but undetectable in *FGFR1*-amplified HCC95 or other lung cancer (H1993, PC-9, EBC1, H1650, H2228, H3122) cells (**Fig. S3A, Table S1**). Notably, synergistic effects of FGFR/PLK1 inhibitors occurred in *FGFR*-amplified cells (H1703, H520, H1581, HCC95) (**Figure 2F, H; Fig. S2A, C**) but not in H522, H226 and HFBN-1 cells despite FGFR1 expression (**Fig. S3A-C**). Moreover, BI2536 in combination with inhibitors targeting other RTKs, such as Afatinib (ERBB) and Erlotinib (EGFR), produced no synergy in H1703 and H520 cells (**Fig. S3D; Table S2**).

Targeting FGFR1 sensitizes breast cancer cells to taxanes (36), a class of anti-mitotic agents. We tested whether similar effects could be observed in *FGFR1*-amplified lung cancer. Paclitaxel, the active ingredient of taxanes, showed weak synergy with the PLK1 inhibitor BI2536 in H520 but not in H1703 cells (**Fig. S3E**). Interestingly, the FGFR inhibitor AZD4547 partially sensitized both cells to Paclitaxel (**Fig. S3E**). These results are consistent with our findings and suggest that the synergistic effects of FGFR/PLK1 inhibition may be due in part to inhibition of PLK1 mitotic function.

Together, these results indicate that PLK1 inhibition potently and selectively enhances the efficacy of FGFR-targeted therapy in *FGFR1*-amplified lung cancer cells.

## **Combined FGFR1/PLK1 inhibition induces cell-cycle arrest and apoptotic cell death by activating the $\gamma$ H2AX-CHK1/2-E2F1 axis**

To investigate the mechanisms underlying combinatorial effects of FGFR and PLK1 inhibition, we first interrogated The Cancer Genome Atlas (TCGA) to determine the cellular processes downstream of FGFR1 signaling. Gene set enrichment analysis (GSEA) of *FGFR1*-amplified H520 and H1581 cells treated with CH5183284/Debio1347, a selective FGFR inhibitor, revealed significant suppression of MAPK (37) and mTORC1 signatures (**Fig. S4A**), which was confirmed by immunoblot analysis in AZD4547-treated H1703 cells (**Figure 2A**; **Fig. S4B**). CH5183284 also significantly blunted DNA damage repair (DDR), G2/M checkpoint, MYC and E2F1 gene signatures (**Figure 3A**; **Fig. S4A**), suggesting a regulatory role by FGFR1 in DDR as well as in MYC- and E2F1-mediated transcriptional programs (2,7,12). Cell cycle analysis showed that FGFR1 inhibition by AZD4547 induced G1 arrest (67.8% by AZD4547 compared to 50.3% by vehicle at 24 h), whereas the PLK1 inhibitor BI2536 arrested the cells at G2/M phase (**Figure 3B**; **Fig. S4C**), consistent with PLK1's roles in cell division (14,16,19). Notably, combination of AZD4547 with BI2536 yielded an even greater G2/M arrest than BI2536 alone, suggesting that PLK1 inhibition can override FGFR1 inhibition-induced G1 arrest, likely through the inactivation of a negative feedback mechanism. Importantly, the drug combination-enabled cell-cycle arrest was paralleled by increased percentage of apoptotic cells (sub-G1) while decreased fraction of G2/M cells in a time dependent manner (**Figure 3B**), suggesting that the FGFR1/PLK1 inhibitor combination-invoked apoptosis might be an ensuing consequence of persistent G2/M cell-cycle arrest. Additionally, our findings indicate that BI2536 treatment abrogates the AZD4547-induced G1 arrest, leading to subsequent accumulation of cells in the G2/M phase.

Next, we performed immunoblot analysis in H1703 cells treated with AZD4547 and BI2536, alone and in combination. Up to 24 h treatment, AZD4547 (5  $\mu$ M) or BI2536 (5 nM) alone hardly affected DNA damage (phosphor-histone H2AX;  $\gamma$ H2AX) and DNA damage responses [p-CHK1 (S345); p-CHK2(T68)] in H1703 cells compared to vehicle, the combination (AZD4547 plus BI2536), however, pronouncedly increased  $\gamma$ H2AX and p-CHK1/2 in a time-dependent manner (**Figure 3C, D**). This increase in DNA damage and DNA checkpoint machinery coincided with strikingly upregulated expression of phosphor-E2F1 [p-E2F1(S364)], phosphor-retinoblastoma protein RB [p-RB(S780)], a negative regulator of E2F1 in G1/S progression (38), and of mitotic [phosphor-histone H3/p-HH3(S10)] and apoptotic markers (cleaved caspase-3 and PARP) (**Figure 3C, D**). These results further support the notion that FGFR1/PLK1 inhibitors-induced apoptosis is a result of prolonged or persistent G2/M arrest.

DNA damage-induced checkpoint activation and the ensuing phosphorylation of E2F1 at the residue serine 364 is a key mechanism prior to initiation of an E2F1-mediated transcriptional program of apoptosis (39-41). To further investigate the causal link between FGFR/PLK1 inhibitors-induced apoptosis and E2F1, we knocked down *E2F1* in H1703 cells. E2F1 downregulation markedly diminished PARP cleavage (Cl PARP) and significantly reduced the percentage of apoptotic subpopulations induced by AZD4547/BI2536 combination (**Figure 3E, F**; **Fig. S4D**), although the treatment successfully upregulated p-CHK2 in *E2F1*-depleted cells (**Figure 3E**).

Together, these results support the notion that concomitant inhibition of FGFR1/PLK1 augments DNA damage accumulation, promotes a G2/M cell-cycle arrest, activates the checkpoint activity and provokes massive apoptotic cell death in an E2F1-dependent manner.

## PLK1 promotes FGFR inhibitor resistance in *FGFR1*-amplified lung cancer

We next determined if PLK1 confers a resistance mechanism to FGFR1 inhibition. To recapitulate the acquired resistance in patients, we generated FGFR inhibitor-resistant cells (H1703R, H520R) by chronic treatment of H1703 and H520 cells with stepwise incremental doses of AZD4547. The resulting H1703R and H520R cells continued to proliferate in the presence of AZD4547 (**Fig. S5A, B**) despite sustained inhibition of FGFR signaling (**Fig. S4B**), suggesting that FGFR inhibition fails to arrest cell cycle progression in the resistant cells, contrary to the pronounced anti-proliferative effect of AZD4547 on parental cells. Immunoblot analysis of H1703R and H520R cells revealed markedly increased expression of PLK1, phosphor-PLK1 [p-PLK1 (Thr210)] that is known to activate PLK1 kinase activity (15,19), and of E2F1 and MYC compared to that in the parental counterparts (**Figure 4A**). Strikingly, while cell cycle-specific inhibitory phosphorylation in RB [p-RB(S780)] was retained in resistant cells, E2F1 was superbly hypo-phosphorylated, as p-E2F1(S364) is hardly detectable despite the abundance of total E2F1. Since RB phosphorylation at serine 780 and E2F1 upregulation are critical for G1/S cell-cycle progression (38), these results provide molecular basis through which H1703R and H520R cells override FGFR inhibition-induced cell-cycle arrest, and further connect PLK1 activation with acquired resistance to FGFR inhibition.

We then tested if PLK1 is functionally associated with FGFR inhibitor resistance. 24 h treatment with BI2536 (5 nM), which precludes PLK1 phosphorylation at threonine 210 and hence inactivates PLK1, markedly increased  $\gamma$ H2AX, p-CHK1 (S345), p-CHK2(T68), p-E2F1(S364) and the cleavage of Caspase-3 and PARP in H1703R and H520R cells although the same treatment only marginally affected these proteins in the parental H1703 and H520 cells (**Figure 4A**). Importantly, H1703R and H520R cells were highly susceptible to PLK1 inhibition, reflected by significantly more pronounced anti-proliferative effects (**Figure 4B, C**) and greater apoptotic cell death induced by BI2536 (5nM) in H1703R and H520R cells than in parental cell lines (**Figure 4D; Fig. S5C**).

Of note, BI2536-provoked increase in DNA damage ( $\gamma$ H2AX) and the ensuing response [p-CHK1 (S345); p-CHK2(T68)] was accompanied by substantially upregulated p-E2F1(S364) although the total E2F1 protein level was largely unchanged (**Figure 4A**), supporting the notion that E2F1 phosphorylation at serine 364 after checkpoint activation (39-41) is important for the induction of apoptosis following PLK1 inhibition. Further confirming a role of E2F1 in PLK1 inhibitor sensitivity, *E2F1* downregulation compromised the effect of PLK1 inhibition, as BI2536 (5 nM) treatment significantly reduced apoptosis in H1703R and H520R cells compared to that in scrambled control siRNAs (**Figure 4E, F**).

Taken together, our data support a model that PLK1 activation restrains E2F1 phosphorylation at serine 364, which abrogates FGFR inhibitor-induced cell cycle arrest and thus promotes FGFR inhibitor resistance (**Figure 4G**). However, concomitant blockage of FGFR1 and PLK1 increases apoptosis through activation of the  $\gamma$ H2AX-CHK1/2-E2F1 signaling axis (**Figure 4G**).

### ***In vivo* efficacy of FGFR/PLK1 combination therapy in *FGFR1*-amplified lung cancer**

Next, we investigated *in vivo* efficacy of combined treatment with FGFR and PLK1 inhibitors using *FGFR1*-amplified lung cancer xenografts and an *FGFR1*-amplified SQLC patient-derived xenograft (PDX; BE973T). H1703 and H520 xenografts were treated with 10 mg/kg body weight, once a day (AZD4547), 40 mg/kg body weight, once a week (BI2536) or 5 mg/kg body weight, once a day (BI6727), all of which are below the clinically achievable doses (21-23,28,42). While AZD4547, BI2536 and BI6727 alone displayed only minor to mild anti-tumor effects compared to vehicle control, drug combinations (AZD4547 plus BI2536 or AZD4547 plus BI6727) demonstrated potent anti-tumor efficacy, resulting in significantly greater suppression of tumor growth than single agents in H1703, H520 xenografts (**Figure 5A-F**) and in the PDX (**Figure 5G-I**). Notably, none of the combinations caused significant loss of mouse body weights (**Fig. S6A-C**) and no other signs of toxicities were observed during the treatment.

Immunohistochemistry (IHC) analysis revealed that drug combination caused significantly more pronounced DNA damage ( $\gamma$ H2AX) and apoptosis (Caspase-3) but decreased Ki-67 or MYC compared to monotherapies in residual PDX (**Figure 5J, K**) and H1703 tumors (**Fig. S6D, E**), which is in line with the *in vitro* observations (**Figure 3**).

Of note, the combination of AZD4547 with BI6727 showed little beneficial effects compared with single agents in *FGFR1* wild-type lung cancer xenografts (EBC-1) (**Fig. S6F-H**), confirming our *in vitro* data (**Fig. S3C**) and further highlighting the superior activity and specificity of combined FGFR/PLK1 inhibitor therapy in *FGFR1*-amplified lung cancer.

### **FGFR and PLK1 pathway alterations are associated with poor outcomes in *FGFR1*-amplified lung cancer patients**

Finally, we addressed the clinical relevance of our findings. Because the combinatorial effect of FGFR1/PLK1 inhibition involves cell-cycle arrest, DNA damage accumulation, and activation of CHK1/2-E2F1 signaling (**Figure 3**; **Fig. S4**), we hypothesized that the related processes regulated by FGFR1 and PLK1 could be of clinicopathological significance for *FGFR1*-amplified lung cancer. Examination of a cohort of patients with SQLC (n=178) in TCGA revealed that, as expected, *FGFR1* gene amplification occurred in a substantial patient subset. In particular, the vast majority of *FGFR1*-amplified SQLC also carried *TP53* mutations (**Figure 6A**), similar to those observed in lung cancer cell lines (**Table S1**). These observations are consistent with the notion that PLK inhibition is effective in p53-deficient setting (19, 20), although further studies are needed to determine exactly how *TP53* mutation status affects response to combined FGFR/PLK1 inhibitor therapy in *FGFR1*-amplified cancers.

Genetic alterations in *PLK1*, *CSNK2A1* (*CK2 $\alpha$* ) and key genes in DNA damage response (*ATR*, *ATM*, *CHEK1/2*), cell-cycle progression (*CCND1*, *CCNE1*, *CDK6*, *MYC* and *E2F1*), and FGFR1 signaling (*AKT1* and *PDK1*) were also detectable in SQLC, independent of *FGFR1* status (**Figure 6A**), suggesting that the significance of these changes in *FGFR1*-amplified lung cancer remains to be explored.

Further analysis of gene expression data of patient-derived *FGFR1*-amplified SQLC revealed that *PLK1* and *FGFR1* expression is negatively correlated (Spearman coefficient: -0.23), in line with our findings that *PLK1* protein level and activity increase upon FGFR inhibition (**Figure 4A**), and with the notion that negative correlation can be exploited to develop rational combination therapies (43). In contrast, *PLK1* is positively correlated with *E2F1* (Spearman coefficient: 0.56), *CSNK2A1* (CK2 $\alpha$ ; Spearman coefficient: 0.37), and *MYC* (Spearman coefficient: 0.30) (**Figure 6B**), consistent with our observation that *PLK1*, *E2F1*, and *MYC* are concomitantly upregulated in FGFR inhibitor-resistant cells (**Figure 3A**). Importantly, *PLK1* is also strongly positively correlated with the expression of key genes involved in HR repair, in particular *RAD51*, *MRE11*, and *BRCA1*, with Spearman coefficient being 0.62, 0.27 and 0.54, respectively, (**Figure 6B**), in favor of a role for *PLK1* to prevent DNA damage accumulation ( $\gamma$ H2AX) in H1703R and H520R cells (**Figure 4A**). These observations are in line with previous studies showing that *PLK1* is causally associated with DDR (15-18) and lend further support for our *in vitro* results indicating that *PLK1* is critical for withholding DNA damage responses upon FGFR inhibition (**Figure 3, 4**).

We finally analyzed the prognostic role of *FGFR1/PLK1* pathway alterations in patients. While high *FGFR1* mRNA expression is associated with better survival in SQLC patients (**Fig. S7**), *FGFR1* amplification predicts poor survival in pan-cancer including SQLC (44), reinforcing the oncogenic significance of *FGFR1* amplification (2,3). *PLK1* is strikingly overexpressed in SQLC compared to normal lung tissues (**Figure 6C**), and high *PLK1* level is correlated with dismal prognosis and increased recurrence rates in patients with *FGFR1*-amplified SQLC and pan-cancers (**Figure 6D, E**). Moreover, elevated *MYC* and *E2F1* expression demonstrated a strong tendency towards poorer survival in patients with SQLC harboring *FGFR1* amplifications, although not of statistical significance due to the small cohort of limited patient number (n=87) (**Figure 6F**). The prognostic value of *FGFR1/PLK1* pathway alterations is consistent with our *in vitro* and *in vivo* results, suggesting the clinical relevance of these findings.

Collectively, the present study establishes a previously unappreciated rationale of combined *FGFR1* and *PLK1* inhibitor therapy for the treatment of *FGFR1*-amplified lung cancer. Given the prevalence of aberrant FGFR signaling in lung and other types of cancer and the advance of *FGFR1* and *PLK1* inhibitors in clinical trials, our work supports further clinical investigations of the new synergistic drug combination in patients harboring *FGFR1*-amplified lung and, perhaps, other cancers.

## DISCUSSION

Despite the prevalence of deregulated FGFR signaling in lung and other cancers, clinical trials with FGFR-TKIs have achieved only limited success in patients with tumors harboring *FGFR* alterations (12,13,42). The broad utility of FGFR-targeted therapies has been limited by their lack of activity in a majority of *FGFR*-altered cancers, as well as acquired resistance of initially responding tumors, suggesting the existence of other auxiliary or compensatory mechanisms that counteract tumor sensitivity to FGFR inhibition. Using an unbiased kinome-wide CRISPR loss of function screen, we identify PLK1 as a previously undescribed synthetic lethal target in *FGFR1*-amplified lung cancer cells treated with FGFR inhibitors. As a result, genetic and pharmacologic inhibition of PLK1 in combination with FGFR-TKIs yields strong synergy, leading to significantly enhanced proliferative inhibition, massively increased apoptotic cell death *in vitro* and potentially augmented anti-tumor efficacy *in vivo*. We further delineate the molecular basis that underpins the combinatorial effect of FGFR/PLK1 inhibition, which involves prolonged G2/M cell-cycle arrest, elevated DNA damage and activation of the pro-apoptotic  $\gamma$ H2AX-CHK1/2-E2F1 signaling.

PLK1 plays pivotal roles in cell-cycle progression by governing mitotic entry and exit (14,19,20). In addition to the canonical role in mitosis, PLK1 also modulates DNA damage responses, as PLK1 can not only promote cell-cycle machinery but also suppress the ATR-CHK1 and ATM-CHK2 checkpoint activity, both of which are required for reactivation or recovery of cell-cycle progression following DNA damage-induced checkpoint arrest (16-18,45). Intriguingly, increasing evidence has also implicated a positive role for PLK1 in DNA damage repair by directly regulating homologous recombination (HR), wherein PLK1 cooperates with CK2 to phosphorylate RAD51, which is necessary for RAD51 recruitment to the site of damage, thereby facilitating HR repair (16,19, 46). These observations suggest that PLK1 can be both a regulator and a downstream factor of DNA damage response, which may represent the two sides of the same coin and can be reconciled after the appreciation of a negative feedback regulation between PLK1 and the DNA damage signaling (17). Our study reinforces the link between PLK1 and DNA damage response, which is supported by several lines of evidence. First, both PLK1 and CK2 $\alpha$  were scored as top candidates in our negative selection CRISPR screen. Secondly, we revealed that acquired resistance to FGFR inhibition is causally associated with PLK1 activation (increased p-PLK1), which is paralleled by repressed double-strand breaks ( $\gamma$ H2AX) and DNA damage checkpoint activity (p-CHK1/2). Thirdly, we demonstrated that PLK1 inhibition acutely upregulates  $\gamma$ H2AX and p-CHK1/2 and induces massive apoptosis in FGFR inhibitor-resistant cells, as did the combination of FGFR1/PLK1 inhibitors in therapy-naïve *FGFR1*-amplified lung cancer cells, which enhances G2/M cell-cycle arrest, DNA damage and significantly increases apoptotic cell death. These findings support a causal contribution to the induction of DNA damage and checkpoint machinery upon PLK1 inhibition, alone (in FGFR inhibitor-resistant cells) and in combination with FGFR-TKIs (in treatment-naïve cells), and, further, are in favor of a model whereby PLK1 inhibition-induced DNA damage is generated as a result of prolonged G2/M arrest (14,20).

Our study implicates a central role for E2F1 in mediating the combinatorial effect of FGFR1/PLK1 targeted therapy. The E2F family of transcription factors regulate the expression

of genes involved in a variety of cellular processes, most prominently cell-cycle progression, DNA damage response and apoptosis (47). A key step leading to E2F1 transcriptional activation and subsequent cell-cycle progression is the phosphorylation of the retinoblastoma (RB) tumor suppressor, which releases E2F1 from the inhibitory binding with RB (38). On the other hand, the involvement of E2F1 in DNA repair is contextually dependent: either as a promoter of cell survival by enhancing DNA damage repair (48) or as a promoter of apoptosis through induction of pro-apoptotic target genes (40). These seemingly dichotomous functions have been proposed to depend on the posttranslational status of E2F1 (49), wherein E2F1-activated apoptosis is specifically preceded by CHK2-mediated phosphorylation of E2F1 at the residue serine 364 (41). In line with such a scenario, we showed that *FGFR1*-amplified lung cancer cells resistant to FGFR inhibition exhibit strikingly upregulated E2F1 that is superbly hypo-phosphorylated at serine 364, while PLK1 inhibition pronouncedly increases the expression of p-CHK1/2 and p-E2F1(S364), concomitant with the induction of massive apoptosis in the resistant cells. Similarly, we demonstrated that apoptosis enabled by combination of FGFR/PLK1 inhibitors is also causally linked with the induction of p-E2F1(S364).

In summary, our work reveals PLK1 as a previously unappreciated therapeutic target whose loss of function is synthetic lethal with FGFR-targeted therapy in *FGFR1*-amplified lung cancer. The molecular basis for the synergy appears to involve the collapse of DNA repair machinery by the combination therapy, which causes greater DNA damage than that achieved by either FGFR1 or PLK1 inhibition alone. Given the clinical advantage of FGFR- and PLK1-targeted agents (12, 19, 20) and the wide prevalence of FGFR alterations in a broad range of human malignancies (1), this rationally derived combination therapy of FGFR/PLK1 inhibitors provides translational potential for treating lung cancer and may be extended to other cancer types with *FGFR* alterations. Importantly, co-targeting FGFR1/PLK1 elicits no additional toxicities beyond that of single drugs in preclinical mouse models, fulfilling the criteria for synergistic combination therapies that are of particular clinical interest due to increased efficacy and selectivity but reduced toxicity (50). Taken together, our findings prioritize further clinical investigations of this newly identified synergistic drug combination in treatment design for patients with *FGFR1*-amplified lung and, perhaps, other cancers as well.

## Acknowledgments

We gratefully acknowledge Lung Cancer Center (LCC), Bern University Hospital and the Tissue Bank Bern (TBB), Institute of Pathology, University of Bern, in acquiring patient tissues. We thank Maja Neuenschwander and Matthias Dettmer (Institute of Pathology) for FISH analysis of FGFR1. We thank Prof. Adrian Ochsenbein, Drs. Carsten Riether and Stefan Forster (Department of Medical Oncology, Bern University Hospital) and Nivia Barontini (Division of Thoracic Surgery, Bern University Hospital) for animal experiments and Prof. Sven Rottenberg (Institute of Animal Pathology, Vetsuisse Faculty, University of Bern) for critical reading of the manuscript. This work was supported by grants from Swiss National Science Foundation (#310030\_192648; to RWP), Swiss Cancer League/Swiss Cancer Research Foundation (#KFS-4851-08-2019; to RWP), Cancer League Bern (to GJK), and PhD fellowships from China Scholarship Council (to ZY, HY, YG, and HD).

## Author contributions

ZY, SQL designed and performed the experiments, analyzed data and wrote the manuscript. HY, DX, RB performed experiments and analyzed data. YG, HD, SB, SRRH, TMM, GJK and QZ analyzed data. RAS provided conceptual inputs and financial support. RWP conceived the project, supervised the study and wrote the paper with support of all co-authors.

## REFERENCES

1. Helsten T, Elkin S, Arthur E, Tomson BN, Carter J, Kurzrock R. The FGFR Landscape in Cancer: Analysis of 4,853 Tumors by Next-Generation Sequencing. *Clin Cancer Res* 2016; 22:259-67.
2. Turner N, Grose R. Fibroblast growth factor signalling: from development to cancer. *Nat Rev Cancer* 2016;10:116-29.
3. Weiss J, Sos ML, Seidel D, Peifer M, Zander T, Heuckmann JM, et al. Frequent and focal FGFR1 amplification associates with therapeutically tractable FGFR1 dependency in squamous cell lung cancer. *Sci Transl Med* 2010;2:62ra93.
4. Heist RS, Mino-Kenudson M, Sequist LV, Tammireddy S, Morrissey L, Christiani DC, et al. FGFR1 amplification in squamous cell carcinoma of the lung. *J Thorac Oncol* 2012;7: 1775-80.
5. Kim HR, Kim DJ, Kang DR, Lee JG, Lim SM, Lee CY, et al. Fibroblast growth factor receptor 1 gene amplification is associated with poor survival and cigarette smoking dosage in patients with resected squamous cell lung cancer. *J Clin Oncol* 2013;31:731-7.
6. Network TCGAR. Comprehensive genomic characterization of squamous cell lung cancers. *Nature* 2012;489:519-25.
7. Brooks AN, Kilgour E, Smith PD. Molecular pathways: fibroblast growth factor signaling: a new therapeutic opportunity in cancer. *Clin Cancer Res* 2012;18:1855-62.

8. Dieci MV, Arnedos M, Andre F, Soria JC. Fibroblast growth factor receptor inhibitors as a cancer treatment: from a biologic rationale to medical perspectives. *Cancer Discov* 2013;3:264-79.
9. Dienstmann R, Rodon J, Prat A, Perez-Garcia J, Adamo B, Felip E, et al. Genomic aberrations in the FGFR pathway: opportunities for targeted therapies in solid tumors. *Ann Oncol* 2014;25:552-63.
10. Guagnano V, Kauffmann A, Wohrle S, Stamm C, Ito M, Barys L, et al. FGFR genetic alterations predict for sensitivity to NVP-BGJ398, a selective pan-FGFR inhibitor. *Cancer Discov* 2012;2:1118-33.
11. Pearson A, Smyth E, Babina IS, Herrera-Abreu MT, Tarazona N, Peckitt C, et al. High-Level Clonal FGFR Amplification and Response to FGFR Inhibition in a Translational Clinical Trial. *Cancer Discov* 2016;6:838-51.
12. Babina IS, Turner NC. Advances and challenges in targeting FGFR signalling in cancer. *Nat Rev Cancer* 2017;17:318-33.
13. Nogova L, Sequist LV, Perez Garcia JM, Andre F, Delord JP, Hidalgo M, et al. Evaluation of BGJ398, a Fibroblast Growth Factor Receptor 1-3 Kinase Inhibitor, in Patients With Advanced Solid Tumors Harboring Genetic Alterations in Fibroblast Growth Factor Receptors: Results of a Global Phase I, Dose-Escalation and Dose-Expansion Study. *J Clin Oncol* 2017;35:157-65.
14. Zitouni S, Nabais C, Jana SC, Guerrero A, Bettencourt-Dias M. Polo-like kinases: structural variations lead to multiple functions. *Nat Rev Mol Cell Biol* 2014;15:433-52.
15. Smits VA, Klompaker R, Arnaud L, Rijksen G, Nigg EA, Medema RH. Polo-like kinase-1 is a target of the DNA damage checkpoint. *Nat Cell Biol* 2000;2:672-6.
16. Takaki T, Trenz K, Costanzo V, Petronczki M. Polo-like kinase 1 reaches beyond mitosis--cytokinesis, DNA damage response, and development. *Curr Opin Cell Biol* 2008;20:650-60.
17. van Vugt MA, Gardino AK, Linding R, Ostheimer GJ, Reinhardt HC, Ong SE, et al. A mitotic phosphorylation feedback network connects Cdk1, Plk1, 53BP1, and Chk2 to inactivate the G(2)/M DNA damage checkpoint. *PLoS Biol* 2010;8:e1000287.
18. Yata K, Lloyd J, Maslen S, Bleuyard JY, Skehel M, Smerdon SJ, et al. Plk1 and CK2 act in concert to regulate Rad51 during DNA double strand break repair. *Mol Cell* 2012;45:371-83.
19. Medema RH, Lin CC, Yang JC. Polo-like kinase 1 inhibitors and their potential role in anticancer therapy, with a focus on NSCLC. *Clin Cancer Res* 2011;17:6459-66.
20. Strebhardt K. Multifaceted polo-like kinases: drug targets and antitargets for cancer therapy. *Nat Rev Drug Discov* 2010;9:643-60.
21. Hofheinz RD, Al-Batran SE, Hochhaus A, Jager E, Reichardt VL, Fritsch H, et al. An open-label, phase I study of the polo-like kinase-1 inhibitor, BI 2536, in patients with advanced solid tumors. *Clin Cancer Res* 2010;16:4666-74.
22. Rudolph D, Steegmaier M, Hoffmann M, Grauert M, Baum A, Quant J, et al. BI 6727, a Polo-like kinase inhibitor with improved pharmacokinetic profile and broad antitumor activity. *Clin Cancer Res* 2009;15:3094-102.
23. Sebastian M, Reck M, Waller CF, Kortsik C, Frickhofen N, Schuler M, et al. The efficacy and safety of BI 2536, a novel Plk-1 inhibitor, in patients with stage IIIB/IV non-small cell lung cancer who had relapsed after, or failed, chemotherapy: results from an open-label, randomized phase II clinical trial. *J Thorac Oncol* 2010;5:1060-7.

24. Steegmaier M, Hoffmann M, Baum A, Lenart P, Petronczki M, Krssak M, et al. BI 2536, a potent and selective inhibitor of polo-like kinase 1, inhibits tumor growth in vivo. *Curr Biol* 2007;17:316-322.
25. Doench JG, Fusi N, Sullender M, Hegde M, Vaimberg EW, Donovan KF, et al. Optimized sgRNA design to maximize activity and minimize off-target effects of CRISPR-Cas9. *Nat Biotechnol* 2016;34:184-91.
26. Shalem O, Sanjana NE, Hartenian E, Shi X, Scott DA, Mikkelsen T, et al. Genome-scale CRISPR-Cas9 knockout screening in human cells. *Science* 2014;343:84-7.
27. Gavine PR, Mooney L, Kilgour E, Thomas AP, Al-Kadhimi K, Beck S, et al. AZD4547: an orally bioavailable, potent, and selective inhibitor of the fibroblast growth factor receptor tyrosine kinase family. *Cancer Res* 2012;72:2045-56.
28. Zhang J, Zhang L, Su X, Li M, Xie L, Malchers F, et al. Translating the therapeutic potential of AZD4547 in FGFR1-amplified non-small cell lung cancer through the use of patient-derived tumor xenograft models. *Clin Cancer Res* 2012;18:6658-67.
29. Xu D, Liang SQ, Yang H, Bruggmann R, Berezowska S, Yang Z, et al. CRISPR Screening Identifies WEE1 as a Combination Target for Standard Chemotherapy in Malignant Pleural Mesothelioma. *Mol Cancer Ther* 2020;19:661-72.
30. Blomen VA, Majek P, Jae LT, Bigenzahn JW, Nieuwenhuis J, Staring J, et al. Gene essentiality and synthetic lethality in haploid human cells. *Science* 2015;350:1092-6.
31. Hart T, Chandrashekhar M, Aregger M, Steinhart Z, Brown KR, MacLeod G, et al. High-Resolution CRISPR Screens Reveal Fitness Genes and Genotype-Specific Cancer Liabilities. *Cell* 2015;163:1515-26.
32. Mackey AM, Sarkes DA, Bettencourt I, Asara JM, Rameh LE. PIP4kgamma is a substrate for mTORC1 that maintains basal mTORC1 signaling during starvation. *Sci Signal* 2014;7:ra104.
33. Singleton KR, Hinz TK, Kleczko EK, Marek LA, Kwak J, Harp T, et al. Kinome RNAi Screens Reveal Synergistic Targeting of MTOR and FGFR1 Pathways for Treatment of Lung Cancer and HNSCC. *Cancer Res* 2015;75:4398-06.
34. Keller DM, Zeng X, Wang Y, Zhang QH, Kapoor M, Shu H, et al. A DNA damage-induced p53 serine 392 kinase complex contains CK2, hSpt16, and SSRP1. *Mol Cell* 2001;7:283-92.
35. Rabalski AJ, Gyenis L, Litchfield DW. Molecular Pathways: Emergence of Protein Kinase CK2 (CSNK2) as a Potential Target to Inhibit Survival and DNA Damage Response and Repair Pathways in Cancer Cells. *Clin Cancer Res* 2016;22:2840-7.
36. Giordano A et al. Polo-like kinase 1 (Plk1) inhibition synergizes with taxanes in triple negative breast cancer. *PLoS One* 2019;14:e0224420.
37. Nakanishi Y, Mizuno H, Sase H, Fujii T, Sakata K, Akiyama N, et al. ERK Signal Suppression and Sensitivity to CH5183284/Debio 1347, a Selective FGFR Inhibitor. *Mol Cancer Ther* 2015;14:2831-9.
38. Bertoli C, Skotheim JM, de Bruin RA. Control of cell cycle transcription during G1 and S phases. *Nat Rev Mol Cell Biol* 2013;14:518-28.
39. Carnevale J, Palander O, Seifried LA, Dick FA. DNA damage signals through differentially modified E2F1 molecules to induce apoptosis. *Mol Cell Biol* 2012;32:900-12.
40. Lazzarini Denchi E, Helin K. E2F1 is crucial for E2F-dependent apoptosis. *EMBO Rep* 2005;6:661-8.

41. Stevens C, Smith L, La Thangue NB. Chk2 activates E2F-1 in response to DNA damage. *Nat Cell Biol* 2003;5:401-9.
42. Paik PK, Shen R, Berger MF, Ferry D, Soria JC, Mathewson A, et al. A Phase Ib Open-Label Multicenter Study of AZD4547 in Patients with Advanced Squamous Cell Lung Cancers. *Clin Cancer Res* 2017;23:5366-73.
43. Sun C, Fang Y, Yin J, Chen J, Ju Z, Zhang D, et al. Rational combination therapy with PARP and MEK inhibitors capitalizes on therapeutic liabilities in RAS mutant cancers. *Sci Transl Med* 2017;9:eaal5148.
44. Kim HR, Kim DJ, Kang DR, Lee JG, Lim SM, Lee CY, et al. Fibroblast growth factor receptor 1 gene amplification is associated with poor survival and cigarette smoking dosage in patients with resected squamous cell lung cancer. *J Clin Oncol* 2013;31:731-7.
45. Shaltiel IA, Krenning L, Bruinsma W, Medema RH. The same, only different - DNA damage checkpoints and their reversal throughout the cell cycle. *J Cell Sci* 2015;128:607-20.
46. Rabalski AJ, Gyenis L, Litchfield DW. Molecular Pathways: Emergence of Protein Kinase CK2 (CSNK2) as a Potential Target to Inhibit Survival and DNA Damage Response and Repair Pathways in Cancer Cells. *Clin Cancer Res* 2016;22:2840-7.
47. Ren B, Cam H, Takahashi Y, Volkert T, Terragni J, Young RA, et al. E2F integrates cell cycle progression with DNA repair, replication, and G2/M checkpoints. *Genes Dev* 2002;16:245-56.
48. Choi EH, Kim KP. E2F1 facilitates DNA break repair by localizing to break sites and enhancing the expression of homologous recombination factors. *Exp Mol Med* 2019;51:1-12.
49. Biswas AK, Johnson DG. Transcriptional and nontranscriptional functions of E2F1 in response to DNA damage. *Cancer Res* 2012;72:13-7.
50. Lehár J, Krueger AS, Avery W, Heilbut AM, Johansen LM, Price ER, et al. Synergistic drug combinations tend to improve therapeutically relevant selectivity. *Nat Biotechnol* 2009;27:659-66.

## FIGURE LEGENDS

### **Figure 1. CRISPR/Cas9 knockout screens to identify synthetic lethal targets in *FGFR1*-amplified lung cancer cells treated with the *FGFR* inhibitor AZD4547.**

**A**, Schematic of the timeline and experimental procedures of CRISPR/Cas9 screen using a pooled sgRNA library targeting the human kinome.

**B**, Box plots of  $\log_2$ -transformed sgRNA normalized read counts from H520 cells prior to drug treatment (baseline), after 21-day treatment with vehicle (Vehicle) or AZD4547 (AZD4547), with experimental replicates (n=3) indicated (Baseline\_1/2/3, Vehicle\_1/2/3 and AZD4547\_1/2/3).

**C**, Scatterplots showing  $\log_2$ -transformed sgRNA normalized read counts of AZD4547- versus Vehicle-treated H520 cells, with sgRNAs targeting *PIP4K2C*, *PLK1* and *CSNK2A1* highlighted. While *PIP4K2C* is a substrate of mTOR previously shown to be a synthetic lethal partner with *FGFR1*, *PLK1* and *CSNK2A1* (encoding *CK2 $\alpha$* ) have been reported to function in the same process (DNA damage repair), highlighting the potential of *PLK1* and *CSNK2A1* as novel synthetic lethal genes with *FGFR1*.

**D**, Frequency histograms showing the top screen hits (n=7; ranked by  $\log_2$ FC) negatively selected in vehicle vs. baseline (left) and AZD4547 vs. vehicle (right) after day 21. Individual sgRNAs targeting the indicated genes are highlighted by red lines, with the  $\log_2$ FC and p values indicated.

**Figure 2. Genetic and pharmacological antagonism of PLK1 plus FGFR inhibitors synergistically suppresses proliferation and enhances apoptosis in *FGFR1*-amplified lung cancer cells.**

**A**, Immunoblots of H1703 and H520 cells treated for 2 h with AZD4547 as indicated concentration.

**B**, Immunoblots of H1703 and H520 cells transfected with *PLK1*-specific siRNAs (si-*PLK1*) or scramble control siRNAs (si-Control).

**C**, Dose-response curves of H1703 and H520 cells expressing *PLK1* or control siRNAs to AZD4547. Cell proliferation was assayed 72 h after drug treatment (84 h after siRNA transfection). Data are presented as mean of three independent experiments (n=3).

**D**, H1703 and H520 cells expressing *PLK1* or control siRNAs were treated with AZD4547 for 72 h and cultured in drug-free medium for additional 7–14 days. Surviving cells after the treatment were fixed and visualized by crystal violet staining. Representative images of three independent experiments (n=3) are shown.

**E**, H1703 and H520 cells expressing *PLK1* or control siRNAs were treated with AZD4547 for 72 h before analyzed by apoptotic assay. Data are presented as mean  $\pm$  s.d. (n=3). \*\* $P < 0.005$  and \*\*\*\* $P < 0.0001$  by two-way ANOVA with Tukey's multiple comparisons test. ns, not significant.

**F-I**, The *PLK1* inhibitor BI2536 synergistically enhances the anti-proliferative effect of AZD4547 in *FGFR1*-amplified lung cancer cells. H1703 and H520 cells treated for 72 h with AZD4547 and BI2536, alone or in combination, were subjected to proliferation analysis (F, H) and clonogenic assay (G, I). The plot of fraction affected (Fa) and combination index (CI) are shown underneath, with  $CI < 1.0$  indicating synergistic effect. The heatmap (F and H; right) indicates the percentage of viable cells after the treatment, based on quantification of clonogenic results (right). Data are presented as mean  $\pm$  s.d. (n=3). \*\*\* $P < 0.001$ ; \*\*\*\* $P < 0.0001$  by two-way ANOVA and Tukey's post hoc test.

**J, K**, H1703 (J) and H520 (K) cells treated with the indicated drugs for 24, 48 and 72 h were subjected to flow cytometry-based apoptosis assay. Data are presented as mean of three independent experiments (n=3).

**Figure 3. Combined FGFR and PLK1 inhibition enhances G2/M arrest and DNA damage-induced apoptosis by activating the CHK2/E2F1 axis.**

**A**, Gene set enrichment analysis (GSEA) of H520 and H1581 cells treated with CH5183284/Debio 1347, a selective FGFR inhibitor. Transcriptomic gene expression data are based on the GEO dataset GSE73024.

**B**, Cell cycle analysis of H1703 cells treated with AZD4547 (5  $\mu$ M) and BI2536 (5 nM), alone or in combination, for 24, 48 and 72 hours. Data are presented as mean of three independent experiments (n=3).

**C**, Immunoblots of H1703 cells treated with vehicle (DMSO), AZD4547 and BI2536, alone or in combination, for 6 h and 24 h.

**D**, Immunofluorescence of H1703 cells treated with vehicle (DMSO), AZD4547 (5  $\mu$ M) and BI2536 (5 nM), alone or in combination, for 24 h. Cells were subsequently stained with antibodies against  $\gamma$ H2AX (Red) and pHH3 (Green) and DAPI (blue; nuclei). Scale bar (white): 25  $\mu$ m.

**E**, Immunoblots of H1703 cells transfected with *E2F1* or control siRNAs and subsequently treated with vehicle (-) or AZD4547 (5  $\mu$ M) plus BI2536 (5 nM) for 24 h.

**F**, H1703 cells transfected with *E2F1* or control siRNAs were treated with vehicle (DMSO), AZD4547 (5  $\mu$ M), BI2536 (5 nM) and the drug combination for 48 h and subsequently analyzed by apoptotic assay. Data are presented as mean  $\pm$  s.d. (n=3). \*\*\* $P$ <0.001 by two-way ANOVA with Tukey's multiple comparisons test.

#### Figure 4. PLK1 promotes acquired resistance to FGFR-targeted therapy.

**A**, Immunoblots of AZD4547-resistant (H1703R, H520R) and parental (H1703, H520) cells after 24 h treatment with vehicle or the PLK1 inhibitor BI2536 (5 nM).

**B, C**, Dose-response curves (upper) and clonogenic assay (middle and bottom) of AZD4547-resistant (H1703R, H520R) and parental (H1703, H520) cells to BI2536. Cells were treated for 72 h before subjected to proliferation and clonogenic assay. Data are presented as mean  $\pm$  s.d. (n=3), with representative results and quantification of clonogenic assay shown. \* $P$ <0.05, \*\* $P$ <0.001, \*\*\* $P$ <0.0001 and \*\*\*\* $P$ <0.00001 by one-way ANOVA with Tukey's multiple comparisons test.

**D**, AZD4547-resistant (H1703R, H520R) and parental (H1703, H520) cells treated for 72 h with BI2536 (5 nM) were analyzed by flow cytometry-based apoptosis assay. The percentage of apoptotic cells was determined by the ratio of apoptotic populations (Annexin V<sup>+</sup>/PI<sup>-</sup> plus Annexin V<sup>+</sup>/PI<sup>+</sup>) versus the total cells. Data are presented as mean  $\pm$  s.d. (n=3). \* $P$ <0.01 and \*\*\*\* $P$ <0.001 by one-way ANOVA with Tukey's multiple comparisons test.

**E**, Immunoblots of H1703R and H520R cells transfected with *E2F1* or control siRNAs.

**F**, H1703R and H520R transfected with *E2F1* or control siRNAs were treated with BI2536 (5 nM) for 72 h and subsequently analyzed by apoptotic assay. Data are presented as mean  $\pm$  s.d. (n=3). \* $P$ <0.01 and \*\* $P$ <0.005 by one-way ANOVA with Tukey's multiple comparisons test.

**G**, Schematic diagram depicting the findings of this study. PLK1 activation promotes DNA damage repair (DDR) and restrains CHK2 and E2F1 phosphorylation, which compensates for FGFR inhibition-induced cell-cycle arrest (left). However, combined FGFR1/PLK1 inhibition induces DNA damage, leading to the induction of CHK2 and E2F1 phosphorylation and in turn apoptosis.

**Figure 5. Combined FGFR and PLK1 targeted therapy potentially inhibits *FGFR1*-amplified lung cancer xenografts.**

**A, B,** Growth curve of H1703 (A) and H520 (B) xenografts treated with vehicle, AZD4547 (10 mg/kg/day), BI2536 (40 mg/kg/week) or BI6727 (5 mg/kg/day), alone and in combination. Data are shown as mean  $\pm$  s.d.. \*\*\* $P$ <0.001 and \*\*\*\* $P$ <0.0001 by one-way ANOVA with Tukey's multiple comparisons test.

**C-F,** Relative tumor volume (C, D) and weights (E, F) of H1703 and H520 xenografts after the treatment for 22 or 24 days. \* $P$ <0.05 and \*\* $P$ <0.01 by one-way ANOVA with Tukey's multiple comparisons test.

**G,** Growth curve of a *FGFR1*-amplified squamous cell lung carcinoma patient-derived xenograft model (BE937T) treated with vehicle, AZD4547 (10 mg/kg/day), BI6727 (5 mg/kg/day), and the drug combination for the indicated time. Data are shown as mean  $\pm$  s.d.. \*\* $P$ <0.01 by one-way ANOVA with Tukey's multiple comparisons test.

**H, I,** Relative tumor volume (H) and weights (I) of PDX (BE937T) xenografts after the treatment for 21 days. ns, not significant, \* $P$ <0.05 by one-way ANOVA with Tukey's multiple comparisons test.

**J, H & E and IHC analysis ( $\gamma$ H2AX, Caspase-3 and Ki-67) of PDX (BE973T) xenografts after the treatment. Original overall magnification,  $\times$ 400(G), scale bar=200  $\mu$ m.**

**K,** Quantification of the IHC data (J) for the positivity of  $\gamma$ H2AX, Caspase-3 and Ki-67. \* $P$ <0.05, \*\* $P$ <0.01, \*\*\* $P$ <0.001 and \*\*\*\* $P$ <0.0001 by one-way ANOVA with Tukey's multiple comparisons test.

**Figure 6. PLK1 pathway alterations are associated with poor clinical outcomes in *FGFR1*-amplified lung and pan-cancer.**

**A**, Somatic mutations, DNA copy-number changes and mRNA expression of *FGFR1* and *PLK1* pathway genes in squamous lung cell carcinoma (n=178). *TP53* alterations are also shown. Patient samples are arranged in columns (each column representing an individual patient) with genes labeled along rows. Data were downloaded from cBioPortal.

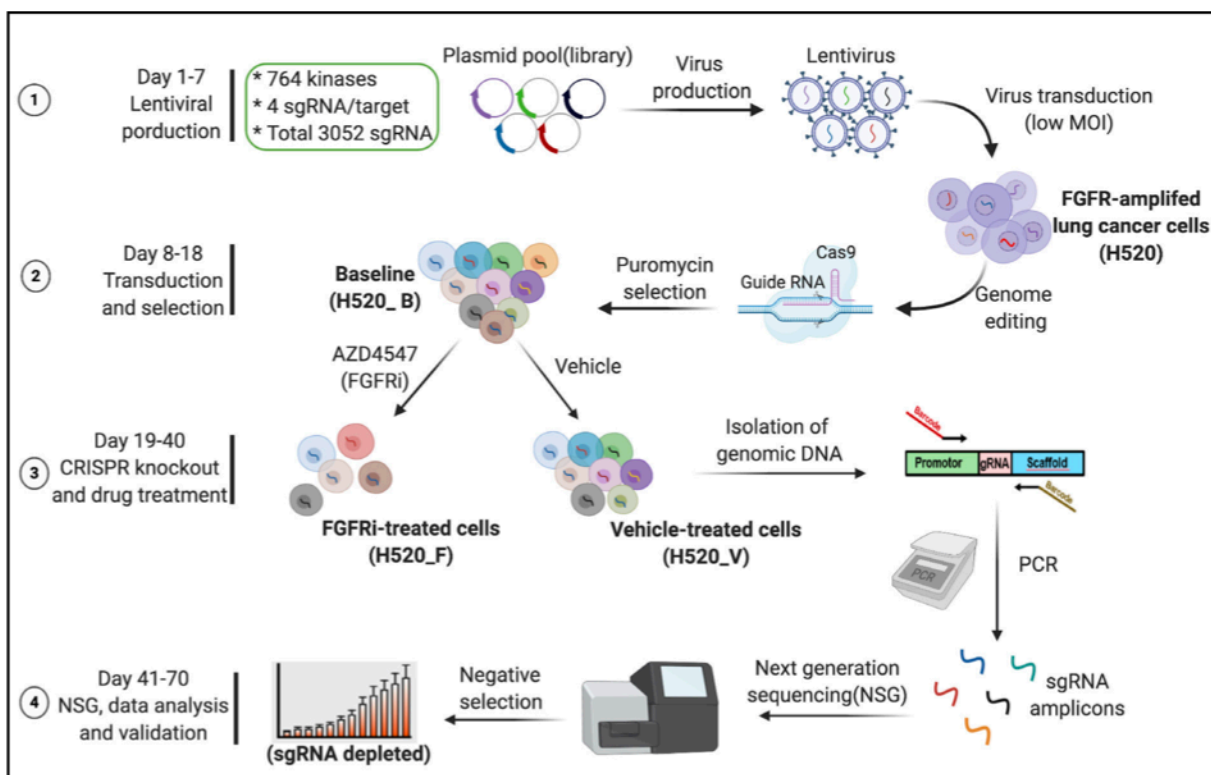
**B**, Correlation analysis of *FGFR1*- and *PLK1*-related genes in patient-derived *FGFR1*-amplified SQLC. Transcriptomic data of a patient cohort (n=36) carrying *FGFR1*-amplified SQLC were downloaded from TCGA. The correlogram (-1 to 1) indicate the correlation coefficient (Spearman). Significant positive (in blue) and negative (in red) correlations are shown, with color intensity proportional to the correlation coefficient. Non-significant correlation is left blank background.  $P < 0.05$  is considered significant.

**C**, *PLK1* expression in SQLC and normal tissue. Transcriptomic data are downloaded from a TCGA cohort of patients with SQLC (n=511). The p-value ( $* < 0.05$ ) was calculated by unpaired student's t-test.

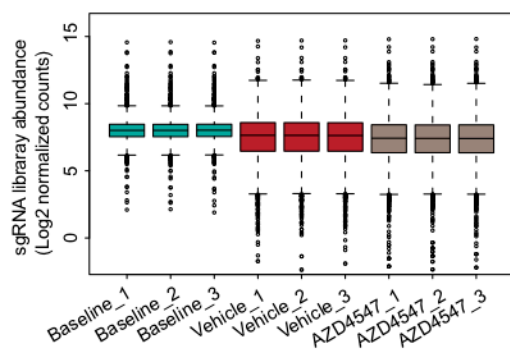
**D, E**, Kaplan-Meier analysis of TCGA cohorts of patients with *FGFR1*-amplified SQLC (D) and *FGFR1*-amplified pan-cancer (E). Stratification of patients into high\_ *PLK1* (in red) and low\_ *PLK1* (in green) is based on the optimal cutoff value of *PLK1* transcripts across all patients by using the `surv_cutpoint` function in R 'maxstat' package. The p-value is calculated using the log-rank test.

**F**, Kaplan-Meier curves showing overall survival (OS) by the gene expression level of *E2F1* and *MYC* based on the optimal cut-off value in a TCGA cohort of patients with *FGFR1*-amplified SQLC. The gene expression and corresponding survival data were extracted for correlation and prognostic analysis using the corresponding packages in R ('corrplot' and 'Hmisc' packages for correlation analysis; 'maxstat', 'survival' and 'survminer' packages for prognostic analysis).

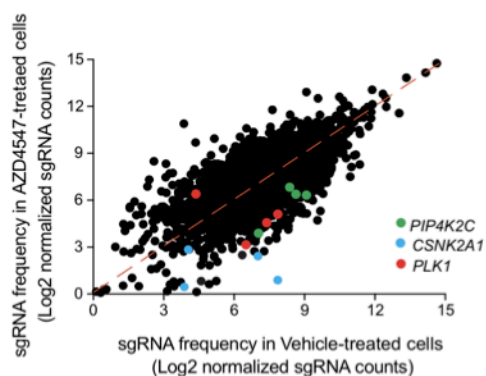
**A**



**B**



**C**



**D**

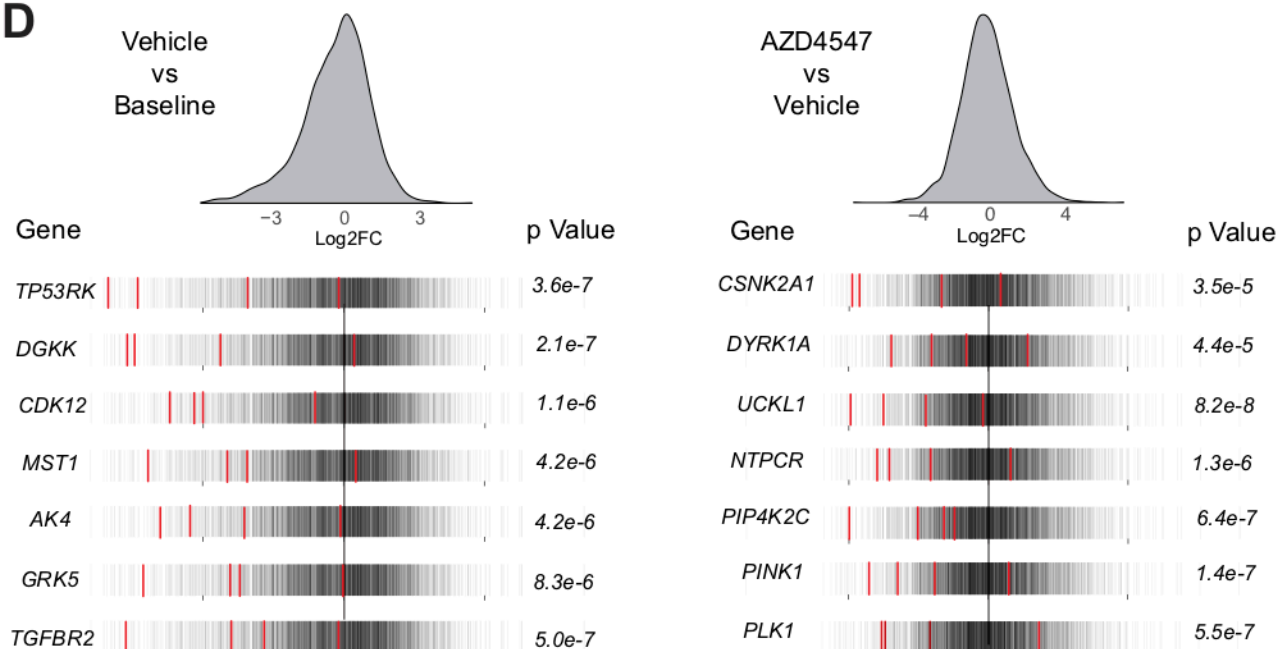
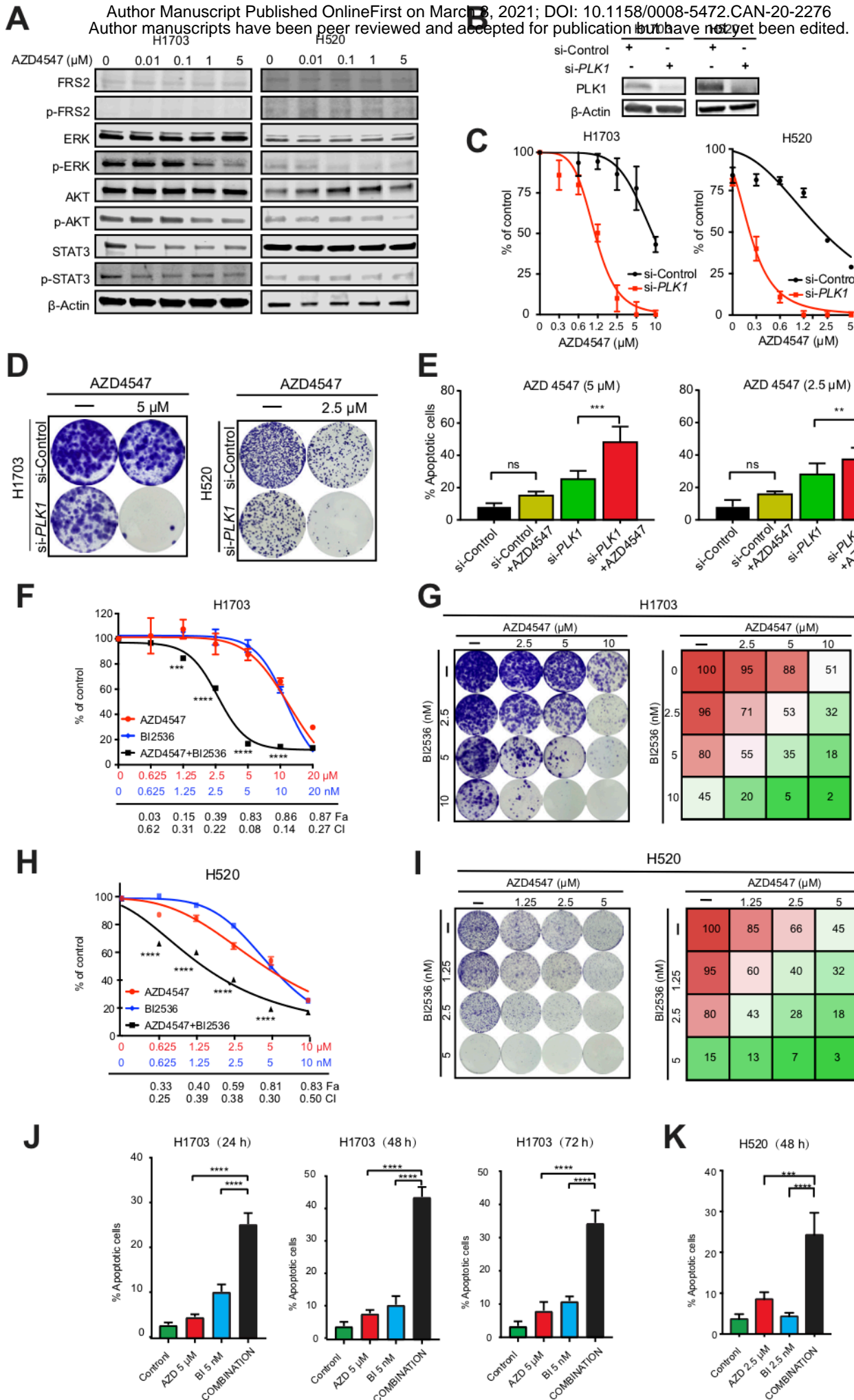
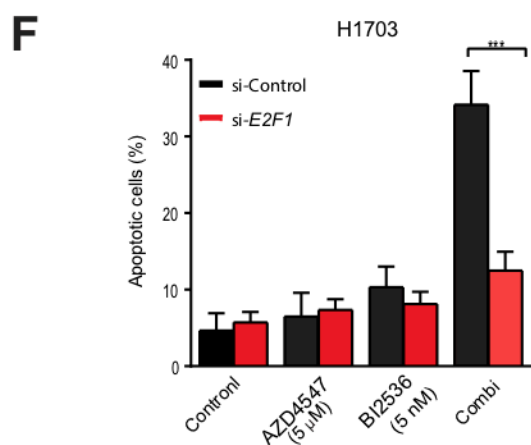
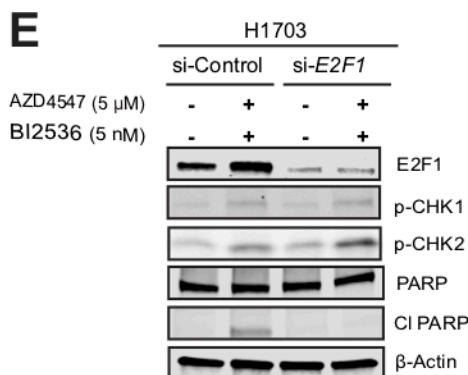
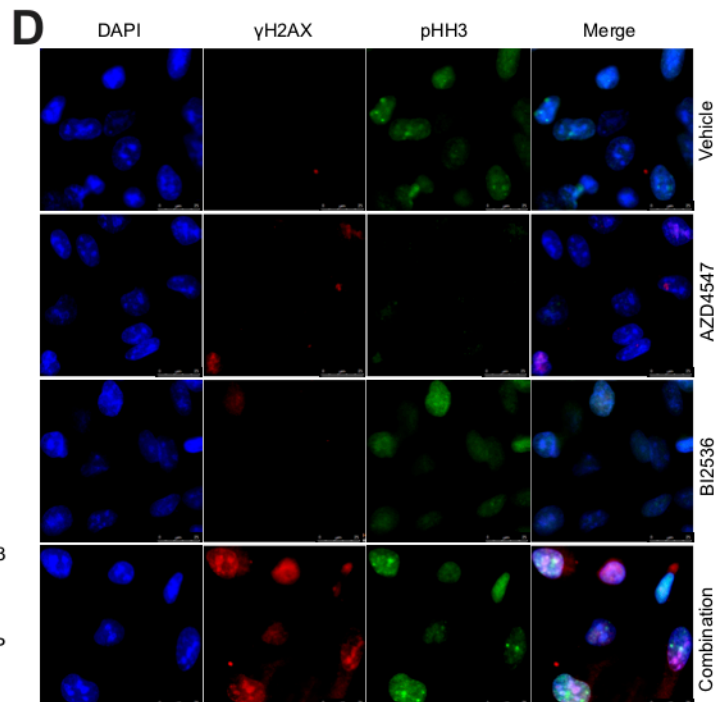
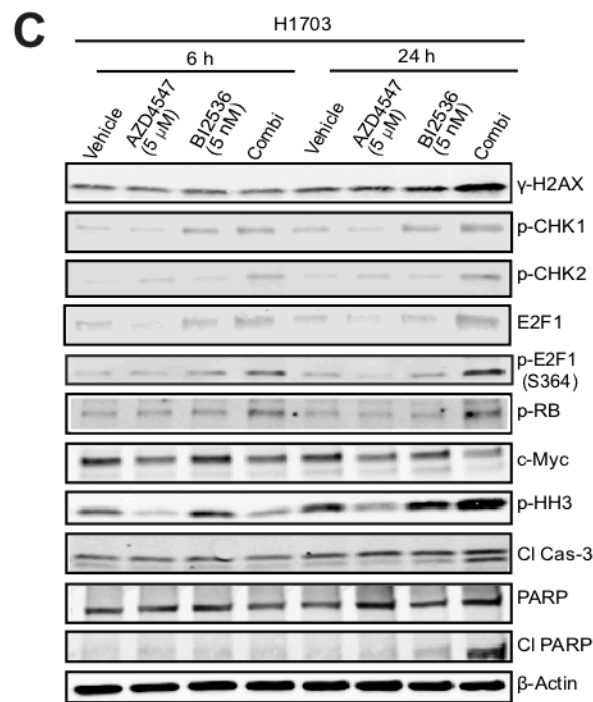
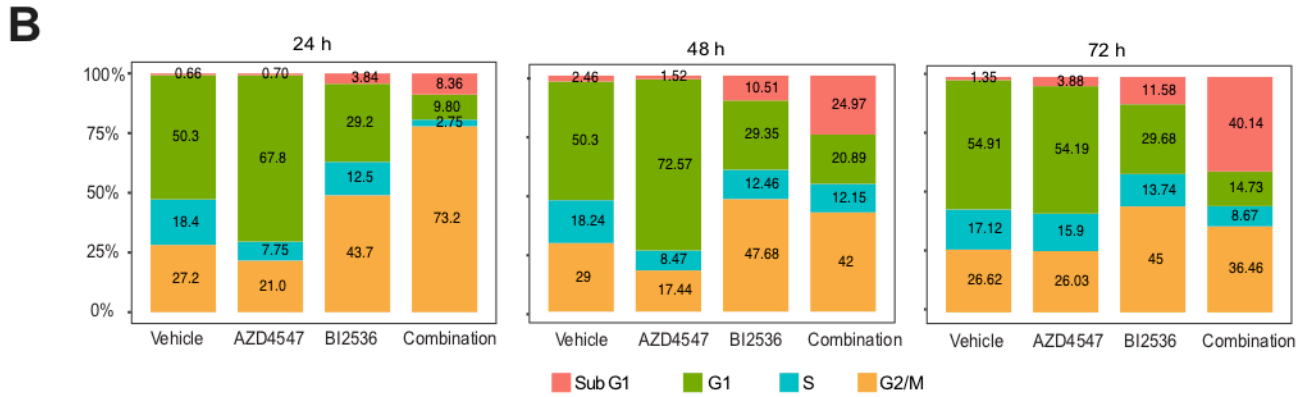
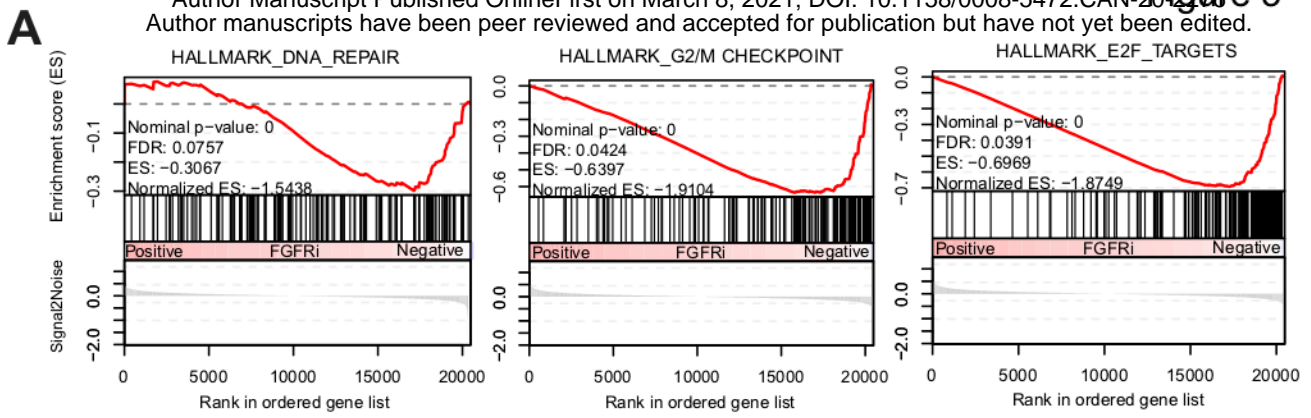
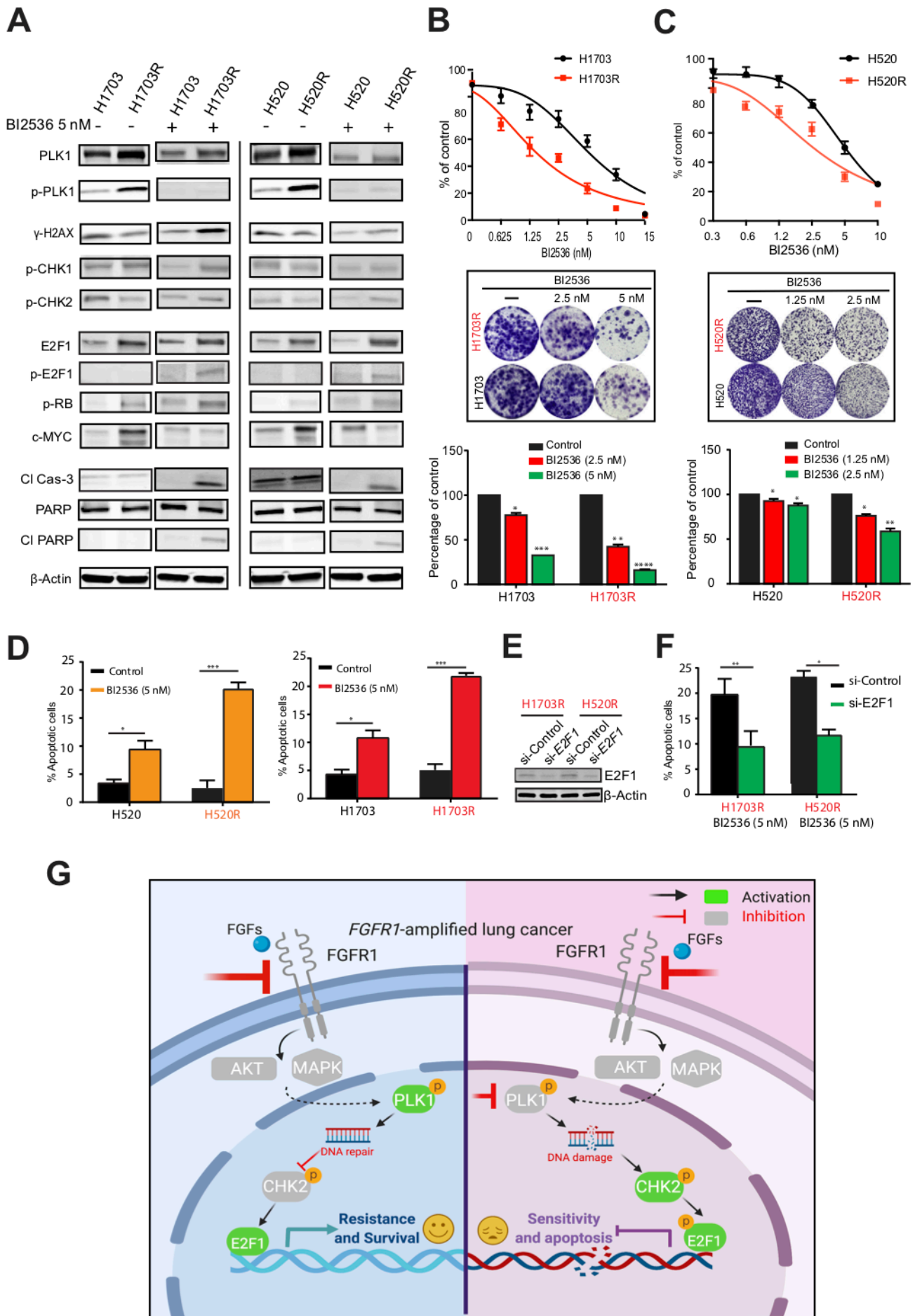
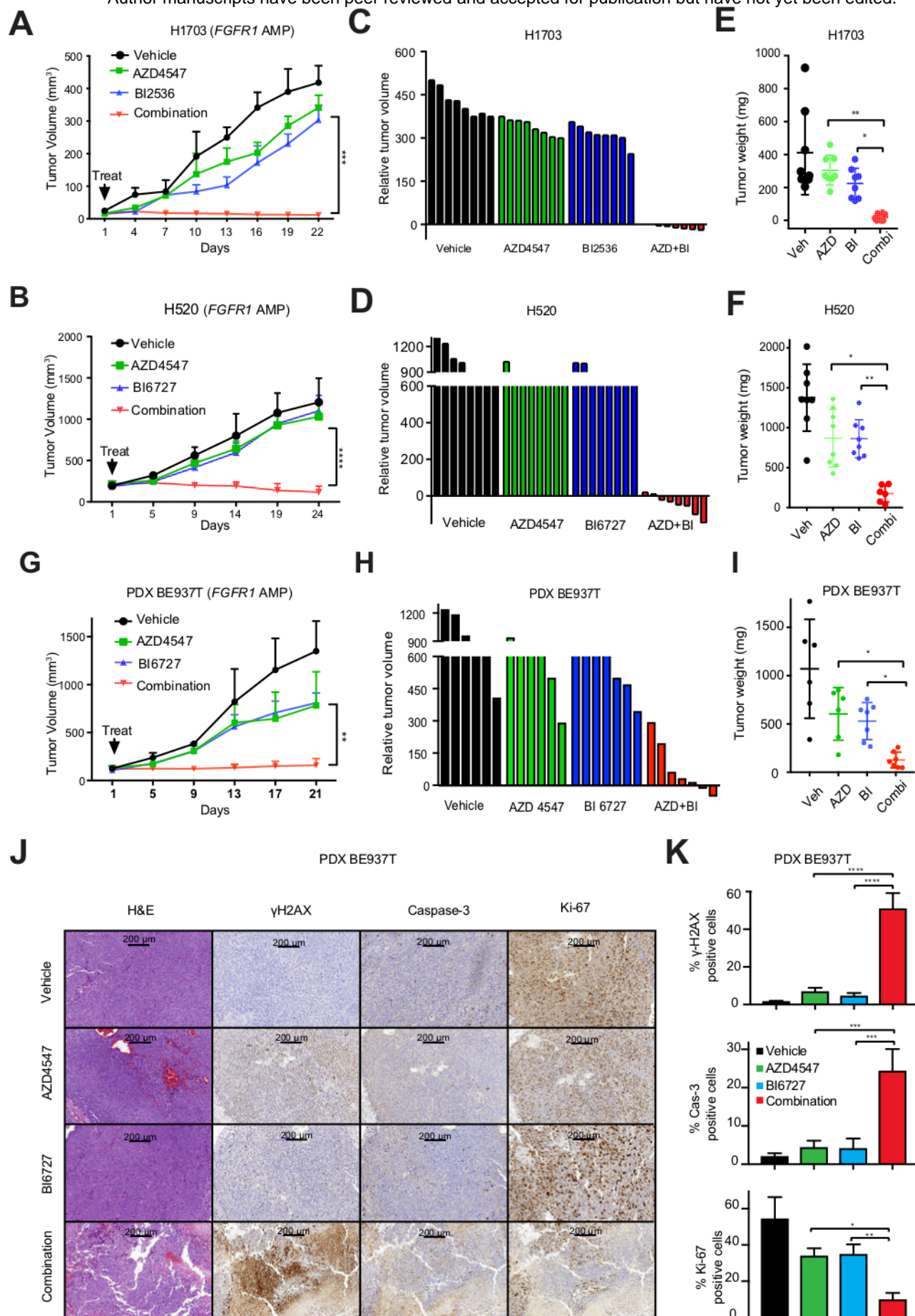


Figure 2



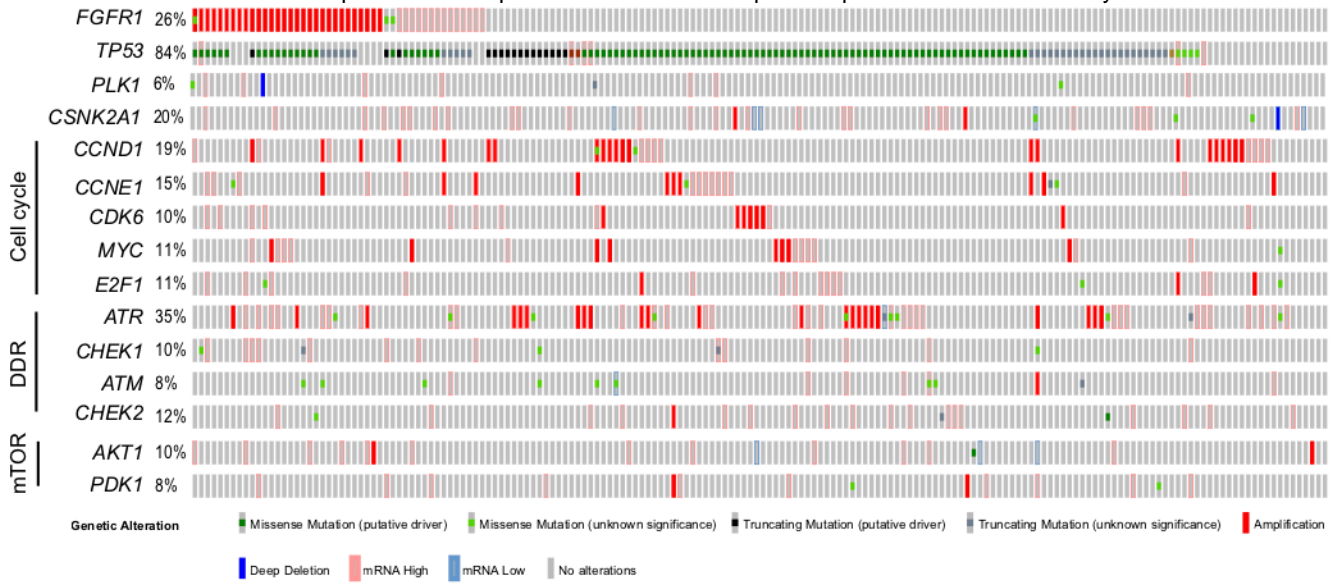




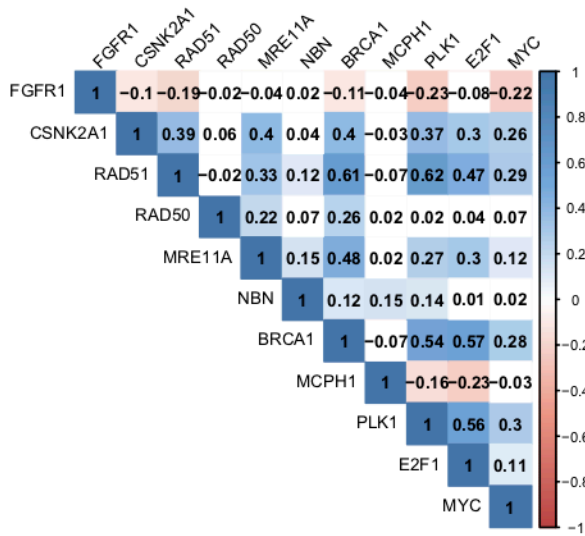


Author manuscripts have been peer reviewed and accepted for publication but have not yet been edited.

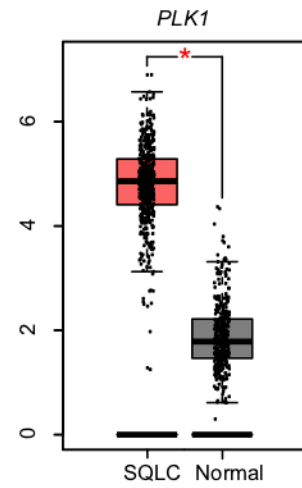
**A**



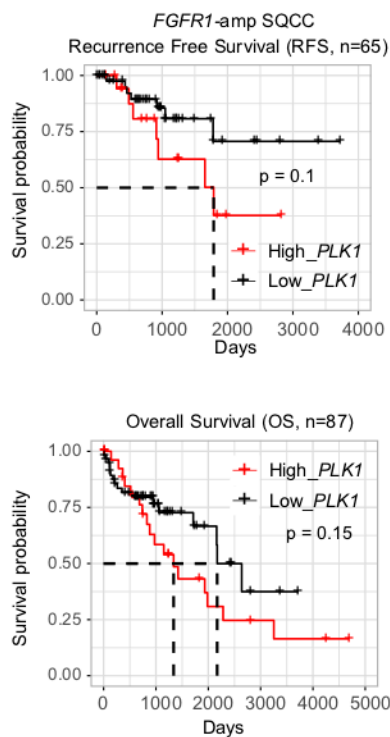
**B**



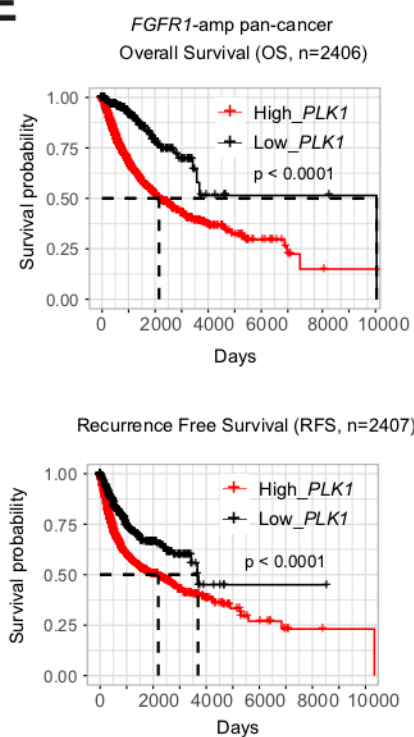
**C**



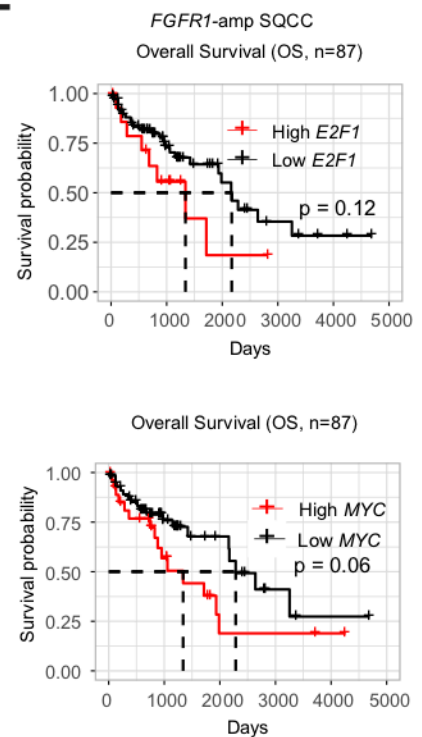
**D**



**E**



**F**



# Cancer Research

The Journal of Cancer Research (1916–1930) | The American Journal of Cancer (1931–1940)

## CRISPR-mediated kinome editing prioritizes a synergistic combination therapy for FGFR1-amplified lung cancer

Zhang Yang, Shun-Qing Liang, Haitang Yang, et al.

*Cancer Res* Published OnlineFirst March 8, 2021.

<b>Updated version</b>	Access the most recent version of this article at: doi: <a href="https://doi.org/10.1158/0008-5472.CAN-20-2276">10.1158/0008-5472.CAN-20-2276</a>
<b>Supplementary Material</b>	Access the most recent supplemental material at: <a href="http://cancerres.aacrjournals.org/content/suppl/2021/03/03/0008-5472.CAN-20-2276.DC1">http://cancerres.aacrjournals.org/content/suppl/2021/03/03/0008-5472.CAN-20-2276.DC1</a>
<b>Author Manuscript</b>	Author manuscripts have been peer reviewed and accepted for publication but have not yet been edited.

**E-mail alerts** [Sign up to receive free email-alerts](#) related to this article or journal.

**Reprints and Subscriptions** To order reprints of this article or to subscribe to the journal, contact the AACR Publications Department at [pubs@aacr.org](mailto:pubs@aacr.org).

**Permissions** To request permission to re-use all or part of this article, use this link <http://cancerres.aacrjournals.org/content/early/2021/03/05/0008-5472.CAN-20-2276>. Click on "Request Permissions" which will take you to the Copyright Clearance Center's (CCC) Rightslink site.